第39卷 第6期 焊 接 学 报 Vol. 39(6):086 -090
2018年6月 TRANSACTIONS OF THE CHINA WELDING INSTITUTION June 2018

微束等离子弧焊三维焊接堆垛过程塌陷

李 挺[1], 黄健康[1], 陈秀娟[2], 杨茂鸿[1], 余淑荣[2], 樊 丁[1]
(1. 兰州理工大学 有色金属先进加工与再利用省部共建国家重点实验室,兰州 730050;
2. 兰州理工大学 机电工程学院,兰州 730050)

摘 要: 采用搭建的三维运动平台对微束等离子弧焊三维焊接堆垛过程中收弧位置塌陷问题进行了研究,利用CCD相机实时跟踪拍摄整个三维焊接堆垛过程,在此基础上分析了堆垛过程中的熔池流动和熔滴过渡变化,并分析了熔池所受作用力及焊接工艺参数对塌陷的影响. 结果表明,收弧位置堆垛墙体下塌是由于被挤压到熔池尾部的液态金属来不及回流以及焊丝最后的熔滴未过渡到熔池中导致填充金属不足、熔覆金属的流淌造成的,且随着堆垛墙体收弧端的下塌量累积,熔滴不能稳定过渡到熔池中,进一步加剧了堆垛墙体在收弧端的塌陷,从而使得三维焊接堆垛过程难以继续.

关键词: 微束等离子弧焊; 三维焊接; 堆垛塌陷
中图分类号: TG 142 文献标识码: A doi: 10.12073/j.hjxb.2018390155

0 序 言

目前,工业零件制造特别是维修零件朝着小批量、用户定制的方向发展,而三维焊接快速成形技术因成本低、可控性好、制造零件致密度高等特点在这一方面具有很大的优势[1]. 微束等离子弧焊(MPAW)与钨极氩弧焊(GTAW)、熔化极气体保护焊(GMAW)相比,其具有更高的电弧挺度、更好的稳定性、更高的电流密度、更小的热影响区、成形后零件残余应力小等优点,因此更适合进行快速成形制造[2]. 当前国内外很多学者对等离子弧焊三维焊接快速成形做了许多相关的研究,文献[3]研究了微束等离子弧焊成形工艺参数对截面宽高比的影响规律并对工艺参数做了优化,发现宽高比大的成形轨迹制造的零件质量更高,而优化参数制造的零件在精度和性能方面都有明显改善. 文献[4]研究了以304L不锈钢为基板的微束等离子弧焊三维焊接快速成形,分析了电流、成形速度与成形轨迹宽度之间的平面几何关系,并发现基于微束等离子弧焊的三维焊接快速成形件的组织结构和力学性能达到或高于铸件. Male等人[5]对不同种类金属的等离子弧焊三维焊接快速成形及试件的性能与熔池的控制做了研究,研究表明非转移型等离子弧可以实现三维焊接快速成形. 徐滨士教授等人[6]研究了脉冲等离子弧焊工艺参数对成形轨迹宽高比及单道成形轨迹宽高比对多道搭接表面平整度的影响规律,发现通过设置合适的层间高度和控制热输入可以有效提高薄壁件的成形精度. 张裕明教授等人[7-8]针对GMAW快速成形中的塌陷现象,提出使焊接电流和成形速度在起弧端从一较大值逐渐过渡到稳定值,收弧端从稳定值逐渐减小的策略,大大减小了塌陷. 但是以上研究都没有涉及到微束等离子弧焊三维焊接堆垛过程中收弧端的塌陷现象. 基于弧焊的三维焊接快速成形在多层单道成形时,收弧位置与中间稳定段的高度尺寸差异逐渐增大,直接影响成形过程的稳定性和成形件的精度,甚至导致成形过程无法继续,而微束等离子弧焊等离子流力大,在堆垛的收弧过程中焊缝的塌陷更为严重,这一现象对薄壁、堆积层高的零件是极为不利的.

三维焊接堆垛塌陷与焊接过程中的熔滴过渡及熔池的流动情况密切相关,因此为了研究微束等离子弧焊三维焊接堆垛塌陷,在所搭建的三维运动平台上进行三维焊接堆垛试验,采用游标卡尺测量堆垛层高度,并采用CCD工业相机实时拍摄整个堆垛过程,分析了中间稳定段和收弧位置的熔滴过渡变化及熔池中液态金属的流动情况,提出了收弧过程中堆垛墙体塌陷的机制.

1 试验方法

微束等离子弧焊三维焊接试验系统如图1所示,主要包括焊接系统、焊接辅助系统、控制系统和

收稿日期: 2017-04-13
基金项目: 国家自然科学基金资助项目(51665034);兰州理工大学红柳青年基金资助项目(Q201202)

视频采集系统四个部分. 其中,焊接系统由 LHM－50 精密微束等离子弧焊机和 WF－007A 多功能自动氩弧填丝机组成; 焊接辅助系统包括三轴数控工作平台、步进电动机等,可以实现三个方向的运动; 控制系统由计算机、CNC 控制器、电机驱动器、工控机、PCL－812PG 数据采集卡、PCL－728 模拟量输出卡和 PCLD－885 固态继电器卡等组成; 视频采集系统由计算机和工业 CCD 相机组成.

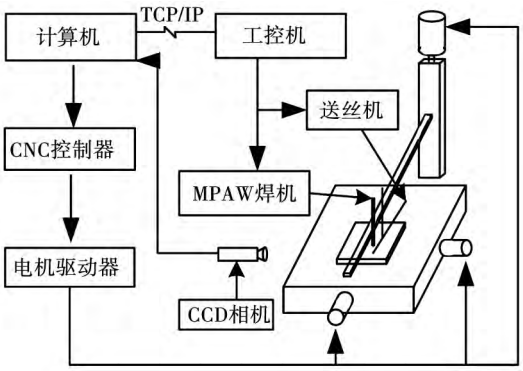

图 1　系统示意图

Fig. 1　Schematic drawing of the system

试验基板选择 304 不锈钢板,尺寸为 200 mm × 100 mm × 3 mm,选用直径为 0.8 mm 的 ER304L 不锈钢焊丝. 试验中堆垛方式采用同向式堆积,如图 2 所示,堆垛方向与送丝方向平行,焊接工艺参数如表 1所示. 在堆垛过程中,用 CCD 工业相机实时跟踪拍摄,最后对拍摄的视频进行分帧,观察分析图片,并且每堆垛一层后用游标卡尺对堆垛高度进行测量.

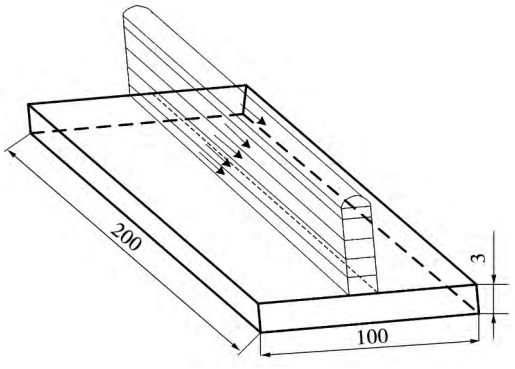

图 2　堆垛路径示意图(mm)

Fig. 2　Schematic drawing of deposition path

表 1　焊接工艺参数

Table 1　Welding parameters

焊接电流 I/A	堆积速度 v_1/(mm·min^{-1})	送丝速度 v_2/(mm·min^{-1})	离子气流量 Q_1/(L·min^{-1})	保护气流量 Q_2/(L·min^{-1})	喷嘴直径 d/mm	层间间隔时间 Δt/s
32	70	800	0.4	6	0.8	90

2　试验结果与分析

2.1　试验结果

为了分析微束等离子弧焊三维焊接堆垛过程中的熔滴过渡变化及熔池流动情况,研究收弧过程中的堆垛塌陷,采用表 1 的焊接工艺参数同向堆垛十七层,并测量了整体堆垛高度,堆垛完成的单墙体形貌和尺寸如图 3 所示. 从图 3a 可以看出,中间稳定段成形良好,收弧端成形不良,具有气孔等缺陷. 相对于中间稳定段,收弧位置高度明显较低,并形成倾斜面. 以测得的整体堆垛高度为纵坐标,以距起弧端的距离为横坐标绘制成图 3b. 从图 3b 中可以看出,收弧端比中间稳定段低约 13 mm. 可以推测,随着堆垛层数的增加,收弧位置相对于中间稳定段的高度差异将越来越大,并且下塌产生的倾斜面逐渐向中间稳定段扩展,使中间稳定段的长度逐渐缩短,最终导致堆垛过程无法继续.

整体高度的差异是由每层的差异累积而成,因此为了分析整体高度差异的变化过程,分别测量了中间稳定段和收弧端各层的堆垛高度,得到图 4 所

(a) 单墙体形貌

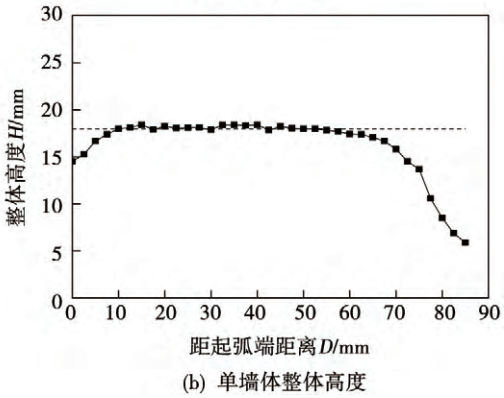

(b) 单墙体整体高度

图 3　单墙体形貌和整体高度

Fig. 3　Forming appearance and total height of single wall

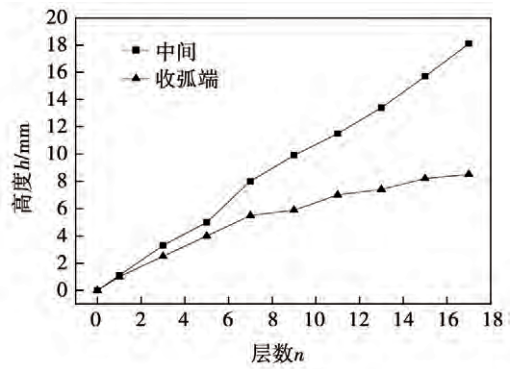

图 4 堆垛高度随层数的变化

Fig. 4 Variation of depositing height with the number of layers

示的堆垛高度随层数的变化关系.

从图 4 中可以看出,中间稳定段堆垛高度随层数的增加基本呈正比例形式均匀增加,收弧端堆垛高度刚开始时增加较快,第七层后增加变缓. 从第三层开始,收弧端的高度与中间稳定段出现明显的差异,之后这种差异越来越大. 这主要是因为堆垛速度和送丝速度等焊接工艺参数恒定,使每层焊缝宽度、金属填充量基本保持不变,焊缝中间稳定段每层高度基本为一定值,而收弧位置,由于散热条件、熔滴过渡等发生变化,不能保持基本恒定的层高,所以随着层数的增加,其与中间稳定段出现明显的差异.

2.2 熔滴过渡分析

在三维焊接堆垛过程中,焊接电流和送丝速度等工艺参数恒定,熔滴能够均匀稳定地过渡到熔池,但是电弧熄灭后,促进熔滴过渡的电磁力等消失,导致最后一滴熔滴未滴下来,如图 5 所示,使收弧位置填充金属减少,冷却后形成凹坑,如图 6 所示.

图 5 收弧位置的熔滴

Fig. 5 Droplet of the end position

随着堆垛层数的增加,收弧位置与稳定段的堆垛高度差逐渐增大,堆垛到收弧端时,焊丝末端与熔池之间距离越来越大,熔滴不能稳定地过渡到熔池,该位置的填充金属进一步减少. 如图 7 所示的收弧位置熔滴过渡,焊丝末端形成的熔滴没有稳定过渡到熔池而是落到熔池之外,通过对分帧图片进行图像处理,发现当焊丝末端距堆垛层 6.40 mm,熔滴直径为 3.84 mm 时,熔滴不能稳定过渡到熔池.

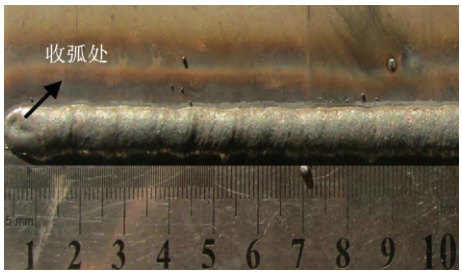

图 6 收弧位置宏观形貌

Fig. 6 Bead appearance of the end position

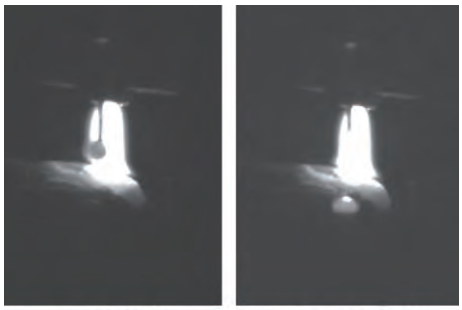

图 7 收弧位置的熔滴过渡

Fig. 7 Droplet transfer of the end position

2.3 熔池流动分析

堆垛高度增加的同时,单墙体收弧位置的散热条件逐渐变差,熔池流动性增强,此外,电弧熄灭后,焊缝尾部的某些地方会产生一个比较大的焊瘤,如图 8 所示,加剧液态金属的流淌.

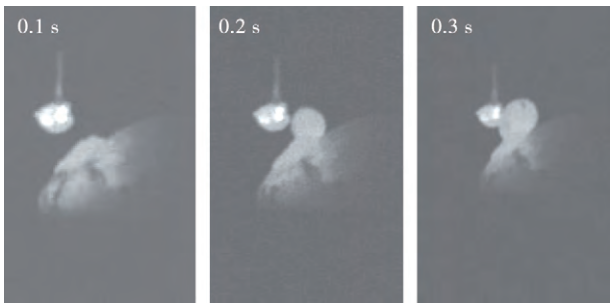

图 8 焊瘤生长形貌

Fig. 8 Growth drawing of the welding beading

在等离子弧焊中,等离子流力、电磁力和重力对焊接熔池流体流动的影响要明显强于表面张力和浮力[9]. 等离子流力的作用使焊接熔池内的液态金属在熔池中心从上向下流动,同时,重力的作用也使熔化的金属从熔池表面向熔池底部运动,而电磁力的作用使液态金属在熔池表面从熔池边缘向熔池中心流动,在熔池内部从熔池中心上部向底部流动,再沿固液界面返回熔池表面.

堆垛时,等离子弧正下方的熔池在上述力的作用下被充分挖掘,在基板或前一层上产生凹坑,并且熔池中的液态金属被挤压到熔池尾部,使熔池呈现倾斜状. 在中间稳定段时,熔敷金属不断补充并且存在固液界面的约束,堆垛层基本保持恒定的高度,如图 9 所示. 而在收弧位置,电弧熄灭后填充金属的补充突然终止,热输入突然消失,被挤压到熔池尾部的液态金属没有足够的时间回流,使收弧位置的熔池继续保持倾斜状,熔池的一边又失去了固液界面的约束,等离子流力、电磁力和重力都有助于液态金属沿倾斜面向下流淌,如图 10 所示,并且随着坡度的增加,这种作用越明显.

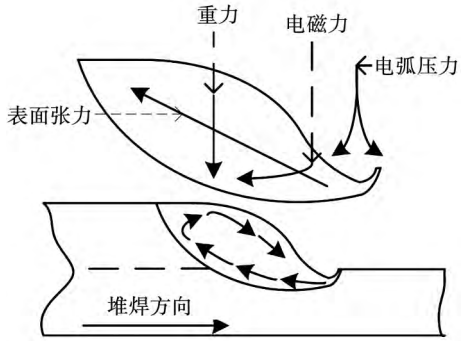

图 9　中部熔池流动行为示意图

Fig. 9　Flow behavior of molten pool in the middle portion of single wall

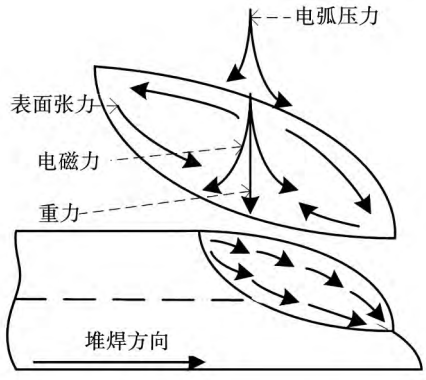

图 10　收弧端熔池流动行为示意图

Fig. 10　Flow behavior of molten pool in the end portion of single wall

3　讨论与展望

焊接过程中,收弧位置的焊缝高度比中间稳定端低,在一般的以连接为目的生产制造中,这一问题并不严重,并且可以通过增加熄弧板有效解决. 但是在弧焊三维快速成形中这一问题非常突出,如果得不到有效的解决,直接影响成形件的精度,甚至由高度不足累计的高度差导致成形过程无法继续. 针对这一问题国内外已有学者做了相关研究,张裕明教授等人[7-8]在同向式堆积时通过将焊接电流和焊接速度在熄弧端逐渐减小的方法改善了这一问题. 张广军教授等人[10-11]在同向式堆积时,在将焊接电流和焊接速度从稳定值逐渐减小的同时增大送丝速度,并在熄弧端使工作平台短暂停留,明显减小了熄弧端与中间稳定段的差异,但是在这种控制策略下,相对于中间稳定段,起弧端略高,熄弧端略低,并且成形效率较低. 同时,他们也研究了交错式堆积方式,运用补偿原理,使第一道焊缝的收弧位置作为第二道焊缝的起弧位置,但是焊接工艺参数恒定. 而这种堆积方式的散热条件差,两端比中间稳定段更差,熔池流动性更强,导致焊缝宽高比增大,两端均比中间稳定段低. 从上述分析可知,影响塌陷的因素主要有焊接电流、焊接速度和送丝速度,因此试验中测量了不同焊接电流、焊接速度及送丝速度下焊缝的熔宽和余高,并计算了焊缝宽高比.

由图 11 可知,随焊接电流的增大,焊缝宽高比逐渐增大,但是增大的速率逐渐减小; 由图 12、图 13 可知,焊缝宽高比随焊接速度的增大逐渐减小,随送丝速度的增大也逐渐减小,并且减小速率均基本保持恒定. 结合焊接电流、焊接速度和送丝速度对焊缝成形的影响规律,分析非封闭路径快速成形中的

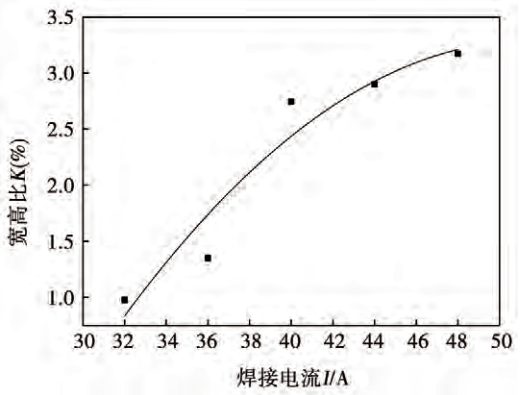

图 11　焊接电流对焊缝宽高比的影响

Fig. 11　Influence of welding current on the ratio of width and height

两种堆积方式,同向式堆积方式在熄弧端停留时,由于端部散热差,熔池流动性强,焊接电流提供的热输入将进一步增强熔池流动性,因此受焊接电流影响较大,不易改进;交错式堆积方式能够以起弧端高出的量补偿前一层熄弧端降低的量,分析认为通过控制起弧和熄弧端的焊接电流及送丝速度,会进一步改善两端较中间稳定段高度不足的问题.

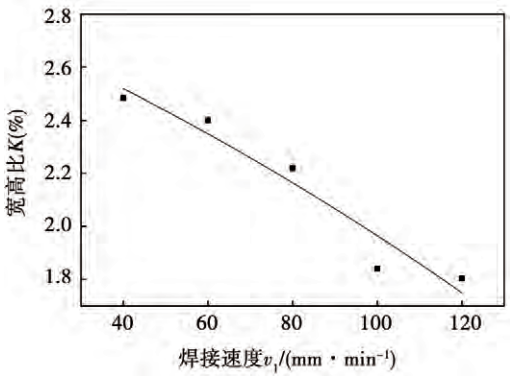

图 12 焊接速度对焊缝宽高比的影响

Fig. 12 Influence of welding speed on the ratio of width and height

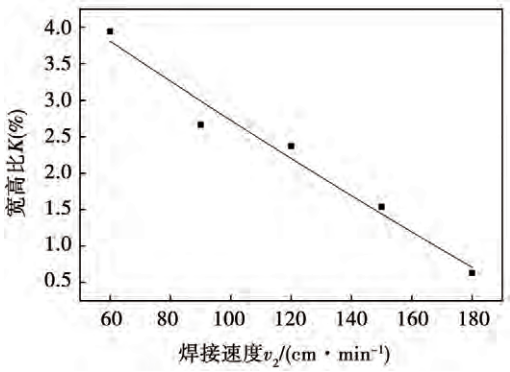

图 13 送丝速度对焊缝宽高比的影响

Fig. 13 Influence of wire feeding speed on the ratio of width and height

4 结 论

(1) 利用 CCD 相机实时跟踪拍摄三维焊接堆垛过程,发现收弧位置塌陷是由熔池中填充金属不足及熔敷金属的流淌造成的,而产生的焊瘤加剧了液态金属的流淌;并且随着堆垛层数的增加,中间稳定段与收弧端的高度差越来越大,熔滴不能稳定过渡到熔池进一步加剧了收弧端的塌陷.

(2) 熔敷金属的流淌主要是由等离子流力、重力和电磁力的作用引起的.

(3) 焊接电流、焊接速度和送丝速度是影响三维快速成形过程中塌陷的主要因素.

参考文献:

[1] Wang H, Kovacevic R. Rapid prototyping based on variable polarity gas tungsten arc welding for a 5356 aluminum alloy [J]. Journal of Engineering Manufacture, 2001, 215(11): 1519 – 1527.

[2] 乌日开西·艾依提, 赵万华, 卢秉恒, 等. 基于脉冲微束等离子弧焊的快速成形系统中实时自适应送丝方式 [J]. 机械工程学报, 2006, 42(1): 181 – 185.
Wurikaixi Aiyiti, Zhao Wanhua, Lu Bingheng, *et al*. Real-time adaptive wire feeding in pulsed micro-plasma arc welding based on rapid prototyping system [J]. Journal of Mechanical Engineering, 2006, 42(1): 181 – 185.

[3] 乌日开西·艾依提, 赵万华, 卢秉恒. 基于微束等离子焊的快速成形中成形参数的优化 [J]. 西安交通大学学报, 2005, 40(5): 568 – 572.
Wurikaixi Aiyiti, Zhao Wanhua, Lu Bingheng. Optimization of process parameters for micro plasma arc welding based rapid prototyping [J]. Journal of Xi'an Jiaotong University, 2005, 40(5): 568 – 572.

[4] 胡晓冬, 彭 伟, 赵万华, 等. 直接金属成形技术的工艺性能研究 [J]. 农业机械学报, 2005, 36(10): 149 – 151.
Hu Xiaodong, Peng Wei, Zhao Wanhua, *et al*. Process properties research for direct metal forming [J]. Transactions of the Chinese Society of Agricultural Machinery, 2005, 36(10): 149 – 151.

[5] Male A T, Chen Y W, Pan C. Rapid prototyping of sheet metal components by plasma-jet forming [J]. Journal of Materials Processing Technology, 2003, 135(2 – 3): 340 – 346.

[6] 徐富家, 吕耀辉, 徐滨士, 等. 基于脉冲等离子焊接快速成形工艺研究 [J]. 材料科学与工艺, 2012, 20(3): 89 – 93.
Xu Fujia, Lü Yaohui, Xu Binshi, *et al*. Study on process of rapid prototyping based on pulsed plasma arc welding [J]. Materials Science and Technology, 2012, 20(3): 89 – 93.

[7] Zhang Y M, Chen Y, Li P, *et al*. Weld deposition-based rapid prototyping: a preliminary study [J]. Journal of Materials Processing Technology, 2003, 135(2 – 3): 347 – 357.

[8] Zhang Y M, Li P, Chen Y, *et al*. Automated system for welding-based rapid prototyping [J]. Mechatronics, 2002, 12(1): 37 – 53.

[9] 马 立. 等离子弧焊接熔池流场与温度场三维数值模拟 [D]. 天津: 天津大学, 2006.

[10] Xiong Jun, Zhang Guangjun, Qiu Zhilong, *et al*. Vision-sensing and bead width control of a single-bead multi-layer part: material and energy savings in GMAW-based rapid manufacturing [J]. Journal of Cleaner Production, 2013, 41: 82 – 88.

[11] Xiong Jun, Zhang Guangjun. Adaptive control of deposited height in GMAW-based layer additive manufacturing [J]. Journal of Materials Processing Technology, 2014, 214: 962 – 968.

作者简介: 李 挺,男,1990 年出生,硕士研究生. 主要从事焊接智能传感与控制研究. Email: liting5936@qq.com

通讯作者: 黄健康,男,博士,副教授,硕士研究生导师. Email: sr2810@163.com

Size effect of solder joints in BGA veneer structure and board-level structure under shear loading JIA Keming, WANG Lifeng, ZHANG Shiyong (School of Material Science & Engineering, Harbin University of Science and Technology, Harbin 150040, China) . pp 67 - 71

Abstract: The shear behavior of solder joints in BGA package structure was studied by test method. The size effect of Sn-3Ag-0.5Cu, Sn-0.3Ag-0.7Cu, Sn-0.3Ag-0.7Cu-0.07La and Sn-0.3Ag-0.7Cu-0.07La-0.05Ce four solder joints were analyzed and compared under the veneer and board-level structure. Results showed: The shear strength of solder joints in the veneer and board-level structure increased with the decrease of the solder joints size, this phenomenon in the solder joints under board-level structure was more obvious. With the decrease of the size of the solder joints, the gap of shear mechanical properties of the low silver solder joints and the high silver solder joints were gradually decreased. The shear strain of the solder joints in the veneer structure increased gradually with the decrease of solder joints size, while the shear strain of the solder joints in the board-level structure was followed by the change law of the first increase and then decrease. In addition, the fracture mode of the high silver solder joints was changed from the mixed-mode of ductile and brittle to the ductile fracture with the size of the solder joint. The fracture mode was unchanged for the other three kinds of low silver solder joints, only the fracture location shifted to the bulk solder.

Key words: size effect; shear properties; veneer structure; board-level structure

Preparation and connection performance analysis of solder paste by low-temperature sintering Cu nanoparticles YANG Wanchun[1], WANG Shuai[2], ZHU Wenbo[1], WEI Jun[1], LI Mingyu[1] (1. School of materials Science and Engineering. Harbin Institute of Technology, Shenzhen Graduate School, Shenzhen 518055, China; 2. Shanghai institute of radio equipment, Shanghai 200090, China) . pp 72 - 76

Abstract: The Cu nanoparticles (Cu NPs) solder paste was applied to connect high-power semiconductor devices at low temperature. The preparation method of the Cu NPs solder paste included the following steps: First, Cu NPs with an average particle size of 30 nm were synthesized by the modified polyol method. Then, the Cu NPs were dispersed in formic acid to remove the surface oxide of Cu NPs. After that, the Cu NPs were mixed with ethylene glycol to prepare solder paste with a solid content of 70%. The DBC ceramic substrate and the metallized SiC die was connected by sintering at low temperature from 160 ℃ to 320 ℃ for 5 min, and the assist pressure was 10 MPa. The morphology of the joint was investigated by scanning electron microscopy (SEM) and transmission electron microscopy (TEM). The result showed that the connection joints with high shearing strength and conductivity were formed by metallurgical bonding between the sintered Cu NPs layer and Cu pad. Coarse microstructure was formed inside the sintered joint.

Key words: Cu nanoparticles; sintering; shear strength; electrical resistivity

Effect of brazing temperature on the interfacial microstructure and mechanical properties of TC4/Ti60 brazed joints NIU Chaonan[1,2], SONG Xiaoguo[1,2], HU Shengpeng[2], FU Wei[1], HAN Linfeng[2], FENG Jicai[1,2] (1. Harbin Institute of Technology, State Key Laboratory of Advanced Welding and Joining, Harbin 150001, China; 2. Harbin Institute of Technology at Weihai, Shandong Provincial Key Laboratory of Special Welding Technology, Weihai 264209, China) . pp 77 - 80

Abstract: In order to study the effect of brazing temperature on the microstructure and mechanical properties of TC4/Ti60 joints, the contact reactive brazing of TC4 and Ti60 alloys using pure copper foil was performed and the brazing temperature ranged from 970 ℃ to 1 010 ℃. The microstructure and mechanical properties of the brazed joints were investigated by scanning electron microscope (SEM), energy dispersive spectrometer (EDS), X-ray diffraction (XRD) and tension shear test. The results showed that the typical interfacial microstructure of TC4/Cu/Ti60 brazed joint was TC4/α-Ti + Ti_2Cu/Ti_2Cu/TiCu/Ti_2Cu/α-Ti + Ti_2Cu/Ti60. The thickness of reaction diffusion layers near substrates were increased with the increasing of brazing temperature, while the width of brazing seam with Ti-Cu intermetallic compounds were decreased. The composition of brazing seam tend to be uniform. The shear strength of joints first increased and then decreased with increasing the brazing temperature. The highest shear strength of 130 MPa was obtained when brazed at 1 000 ℃ for 10 min. Fracture analysis indicated that the quasi-cleavage fracture occurred between the center of brazing seam and the reaction diffusion layer.

Key words: contact reaction brazing; pure copper interlayer; brazing temperature; interfacial microstructure; mechanical properties.

Effect of solution treatment on the microstructure of Inconel 625 alloy fabricated by arc additive manufacturing FENG Yingchao[1], LIU Jinping[1,2], WANG Shijie[1], SUN Qingjie[2], Xu Pengwei[2], LIU Yibo[2] (1. China Nuclear Industry 23 Construction Co. Ltd, Beijing 101300, China; 2. Harbin Institute of Technology at Weihai, Shandong Provincial Key Laboratory of Special Welding Technology, Weihai 264209, China) . pp 81 - 85

Abstract: GTAW additive manufacturing technology was used for fabricating Inconel 625 alloy thin-wall component. Effects of solution treatment on microstructure and mechanical properties were investigated. It was indicated that the fabricated Inconel 625 sample consists of cellular dendritic which grew epitaxially from the substrate. Laves phase and MC-type carbide were also observed in the microstructure of as-welded sample. Compared with as-welded sample, the microstructure after solution treatment at 680 ℃ shows minimal variation, elements Nb, Mo in Laves phase began to spread to the matrix, therefore δ phase was precipitated alongside with Laves phase. With an increase in solution treatment temperature, the amount of dissolved Laves phase and precipitation δ phase increased. At 1 080 ℃, most Laves particles were dissolved into the matrix, Nb, Mo segregation were relieved, remaining small amount of fine particles are dispersed on the matrix.

Key words: additive manufacturing; Inconel 625 alloy; solution treatment; microstructure

Study on the collapse of 3D welding stacking process by micro plasma arc welding LI Ting[1], HUANG Jiankang[1], CHEN Xiujuan[2], YANG Maohong[1], YU Shurong[2], FAN Ding[1]

(1. State Key Laboratory of Advanced Processing and Recycling of Non-ferrous Metals, Lanzhou University of Technology, Lanzhou 730050, China; 2. School of Mechanical and Electronical Engineering, Lanzhou University of Technology, Lanzhou 730050, China) . pp 86 - 90

Abstract: The collapse of three dimensional welding stacking in the end portion of the weld pass was studied by micro plasma arc welding on the 3D motion platform. 3D welding stacking pocess was tracked in real time by using a CCD camera. The change of the weld pool and the droplet transferring were observed and analyzed . The influence of welding force and welding parameters on the collapse was investigated. Experimental results showed that the reasons of the collapse in the end portion of the weld pass include the flow of molten metal and the lack of the filler metal due to the fact the liquid metal pressed to the rear end of the weld pool, which can not be returned and the last molten droplet on the wire is not transfer to the weld pool. Especially, the accumulation of sinking in the end of stacking wall resulted in the droplet not transfer stably to the molten pool, and it makes the collapse further exacerbate. As the result, 3D welding stacking process is hardly continued.

Key words: micro plasma arc welding; 3D welding; stacking collapse

Influence of pin length on formation and shear failure load of dissimilar Al alloys FSLW joint LIU Jian[1], LIU Xuesong[2], XING Yanshuang[1] (1. CSR Qingdao Sifang Co., Ltd., Qingdao 266111, China; 2. State Key Laboratory of Advanced Welding and Joining, Harbin Institute of Technology, Harbin 150001, China) . pp 91 - 95

Abstract: During the experiment dissimilar 2024/7075 Al alloys were friction stir lap welded. The cross sections and lap shear failure loads of lap joints under 3 mm and 4 mm pin lengths were compared. The experimental results showed that the mixing of materials between the upper and lower sheets was heightened with increasing rotational speed of tool. Lower plunge depth of tool pin more easily attained the higher effective sheet thickness and bigger effective lap width. When the rotational speed varied from 800 r/min to 1 200 r/min, the ESTs got by 3 mm pin length decrease firstly then increase with the rotational speed increase, and the ESTs got by 4 mm pin length increase with the rotational speed increase. The maximum shear failure loads of friction stir lap welding joint by 3 mm and 4 mm pin lengths were attained at 800 r/min and 1 200 r/min, respectively. And the values were 10.3 kN and 10.7 kN. The welding lap joints mainly presented tensile fracture mode.

Key words: dissimilar 2024/7075 Al alloys; friction stir lap welding joint; cross section; shear failure load

Texture feature extraction and recognition of magneto-optical images of welded defects based on GLCM-Gabor LAN Chongzhou, GAO Xiangdong, MA Nüjie, ZHANG Nanfeng (Guangdong Provincial Welding Engineering Technology Research Center, Guangdong University of Technology, Guangzhou 510006, China) . pp 96 - 99

Abstract: A nondestructive testing method for welded defects based on texture features of magneto-optical image was studied. The relation between welded defect and magneto-optical image was analyzed by Faraday magneto-optical effect, leak magnetic flux and magnetic domain theory. The texture features were extracted by using GLCM to calculate magneto-optical image. Due to the difference of GLCM texture features between crack and sag was subtle, the texture features of magneto-optical image were further extracted by using Gabor filter. A pattern recognition method based on GLCM-Gabor and SVM was proposed to establish the classification model by processing magneto-optical images of welded defects. Classification result showed that seam features (sag, crack, incomplete penetration and no defect) in surface and subsurface could be recognized by this method with an accuracy rate of 89.7%.

Key words: welded defect; magneto-optical imaging; texture feature; support vector machine

Determination of peak flow rate of the media in oil-gas pipelines for in-service welding YU Chen[1], CHEN Jing[1], CHEN Huaining[1], CHEN Juan[2], ZHANG Manman[2], MA Junhong[2] (1. Key Laboratory of Nuclear Materials and Safety Assessment, Institute of Metal Research, CAS, Shenyang 110016, China; 2. Maintenance & emergency repair Co. of China petroleum pipeline bureau, Langfang 065000, China) . pp 100 - 103, 109

Abstract: Based on the actual working conditions of oil-gas pipelines in-service welding, the simulating calculation of the relationship between the media flow rate and the cooling time $t_{8/5}$ was carried out with finite element method, and the influence factors of $t_{8/5}$ was systematically studied. Referring to the calculation and experimental verification results with the water medium, the influence of the media flow rate and the pipe wall thickness on $t_{8/5}$ were analyzed and the relating formula among them was determined. The results showed that the action of the internal media flow rate on $t_{8/5}$ could be negligible as the pipe wall thickness was greater than 12 mm. In that case, $t_{8/5}$ was mainly controlled by the steel thermal conductivity. The gas pressure had a great impact on $t_{8/5}$, the greater the pressure, the smaller $t_{8/5}$ was. The allowable maximum hardness of difference pipeline steels for in-service welding is closely related with $t_{8/5}$. The peak flow rate for the oil or gas medium was calculated with the gained formula while the value of $t_{8/5}$ related to maximum hardness was determined.

Key words: oil-gas pipelines; in-service welding; peak flow rate; finite element analysis

A smooth trajectory motion control strategy of underwater welding robot XIANG Lintao[1], CHEN Guodong[2], ZHANG Panfeng[3], LU Xiaohui[1] (1. City College of Dongguan University of Technology, Dongguan 523419, China; 2. China Nuclear Power Technology Research Institute Co., Ltd., Shenzhen 518124, China; 3. School of Mechanical and Automotive Engineering, South China University of Technology Guangzhou, Guangzhou 510000, China) . pp 104 - 109

Abstract: In the arc welding process of underwater welding robot, in order to improve the welding quality and the welding efficiency, a smooth trajectory control strategy was presented. Firstly, the mathematical model of the welding robot was established and the kinematics analysis was carried out by using the D-H parameter method. The forward kinematics and inverse kinematics formulas of the robot were deduced and the position formula of the robot was simplified. Then, the 6-dimensional